Imaging and manipulation of the competing electronic phases near the Mott metal-insulator transition

Tae-Hwan Kim[a], M. Angst[b], B. Hu[c], R. Jin[c], X.-G. Zhang[a], J. F. Wendelken[a], E. W. Plummer[c,1], and An-Ping Li[a,1]

[a]Center for Nanophase Materials Sciences, Oak Ridge National Laboratory, Oak Ridge, TN 37831; [b]Materials Science and Technology Division, Oak Ridge National Laboratory, Oak Ridge, TN 37831; and [c]Department of Physics and Astronomy, Louisiana State University, Baton Rouge, LA 70803

Contributed by E. Ward Plummer, February 1, 2010 (sent for review May 20, 2009)

The complex interplay between the electron and lattice degrees of freedom produces multiple nearly degenerate electronic states in correlated electron materials. The competition between these degenerate electronic states largely determines the functionalities of the system, but the invoked mechanism remains in debate. By imaging phase domains with electron microscopy and interrogating individual domains in situ via electron transport spectroscopy in double-layered $Sr_3(Ru_{1-x}Mn_x)_2O_7$ ($x = 0$ and 0.2), we show in real-space that the microscopic phase competition and the Mott-type metal-insulator transition are extremely sensitive to applied mechanical stress. The revealed dynamic phase evolution with applied stress provides the first direct evidence for the important role of strain effect in both phase separation and Mott metal-insulator transition due to strong electron-lattice coupling in correlated systems.

phase separation | electron microscopy | electron transport | scanning tunneling microscopy | strongly correlated materials

It is becoming increasingly clear that the exotic properties displayed by complex materials such as high-T_c superconductivity in cuprates, "colossal" magnetoresistance (CMR) in manganites, and heavy-fermion behavior in f-electron compounds are intimately related to the coexistence of competing nearly degenerate states which couple with active degrees of freedom—charge, lattice, orbital, and spin states (1). The striking phenomena associated with these materials are due in large part to spatial electronic inhomogeneities that can be manifested in electronic phase fluctuations and phase separation (PS) (1–4). While electronic phase fluctuations are difficult to probe due to their dynamic nature, electronic PS and domain percolation have indeed been observed as a function of temperature and magnetic field in manganites, which have led to a breakthrough in understanding the CMR effect (5, 6). Although it has been suggested (7), the interplay between phase separations and mechanical strain has not been directly observed.

Particularly, in d-electron systems where the on-site electron-electron Coulomb repulsion energy U is comparable to the tunneling electron hopping amplitude t or the bandwidth W, a Mott-type metal-insulator transition (MIT) can occur. The ground state of a Mott insulator is usually antiferromagnetic in nature, but can be modified by either charge doping (the band filling) or crystal engineering (the bandwidth control) (1). Near the Mott MIT boundary, competition between different ground states may lead to electronic PS. Various spectroscopic measurements have revealed the competing states and the associated electronic inhomogeneities (8–10), however, the interplay between bandwidth control and electronic PS near the Mott MIT is still unresolved (1, 11, 12).

The correlated electron material studied here is Mn-doped $Sr_3(Ru_{1-x}Mn_x)_2O_7$, which belongs to the Ruddlesden-Popper series with a stacking of two layers of corner-sharing RuO_6 octahedra separated by cation oxide rock-salt layers (13). The ground state of undoped ($x = 0$) $Sr_3Ru_2O_7$ is a Fermi liquid with strong electronic correlations and an exchange-enhanced paramagnetism (PM) (14, 15). The substitution of Ru by Mn strengthens the electron correlation via the modification of the lattice, and the system becomes a Mott insulator at low temperatures (16). According to previous work (16, 17), the Mott MIT occurs with $(5 \sim 20)\%$ Mn doping ($x = 0.05 \sim 0.2$) in $Sr_3(Ru_{1-x}Mn_x)_2O_7$, accompanied with antiferromagnetic (AFM) ordering. Here, we cleave the layered $Sr_3(Ru_{1-x}Mn_x)_2O_7$ single crystals with $x = 0$ and 0.2 in ultrahigh vacuum (UHV) to create a fresh ab plane (see Fig. S1) and investigate in situ their electronic phases using multiple surface analytical techniques. Our results provide real-space images of PS and the evolutions of phase domains with applied mechanical stress and temperature near the Mott MIT boundary of $Sr_3(Ru_{0.8}Mn_{0.2})_2O_7$. The dramatic responses of PS to strain and temperature validate the important role of electron-lattice interactions in PS and confirm the coexistence of competing phases in the vicinity of a Mott MIT, opening up the possibility to manipulate the Mott MIT with stress.

Results and Discussion

Imaging of competing phases was carried out in a cryogenic four-probe scanning tunneling microscope (STM) system (18, 19). This system combines UHV field emission scanning electron microscopy (SEM), STM, and in situ electron transport spectroscopy, providing an unprecedented capability for imaging PS and interrogating individual microscopic domains in real-space and real-time. Striking domain structures are revealed in the $Sr_3(Ru_{0.8}Mn_{0.2})_2O_7$ surface (ab plane) at low temperatures by SEM operated in the secondary electron emission mode. At 81 K, micrometer-scale dark regions with bubble- (Fig. 1A) and stripe-like (Fig. 1B) domains are clearly seen in an otherwise bright matrix of the cleaved surface. However, such domain structure is not revealed at room temperature in the doped compound nor in the undoped compound ($x = 0$) in the measured temperature range of 10–300 K (Fig. 1C). The electronic properties of individual domains are then investigated by scanning tunneling spectroscopy (STS) measurements that probe the integrated density of electronic states near the Fermi energy, E_F. The spatially averaged tunneling $I(V)$ curve taken in the bright regions is markedly different from that in the dark regions, with a strong suppression of current near E_F in the dark regions (Fig. 1D). The derivative of $I(V)$ data (inset of Fig. 1D) reveals an energy gap near E_F in the dark regions for both stripe and bubble domains, in contrast to a finite density of states in the bright

Author contributions: T.-H.K., E.W.P., and A.-P.L. designed research; T.-H.K., M.A., B.H., R.J., J.F.W., and A.-P.L. performed research; T.-H.K., X.-G.Z., and A.-P.L. analyzed data; T.-H.K., R.J., E.W.P., and A.-P.L. wrote the paper.

The authors declare no conflict of interest.

Freely available online through the PNAS open access option.

[1]To whom correspondence may be addressed. E-mail: apli@ornl.gov or eplummer@utk.edu.

This article contains supporting information online at www.pnas.org/cgi/content/full/1000655107/DCSupplemental.

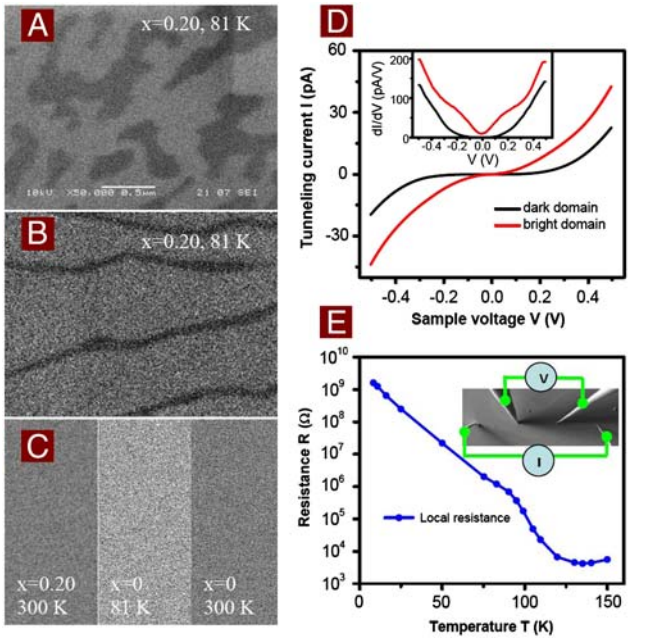

Fig. 1. Electronic phase separations displayed in the cleaved surfaces of $Sr_3(Ru_{1-x}Mn_x)_2O_7$. (*A*), Bubble- and (*B*), Stripe-shaped domain structures revealed by SEM for $x = 0.20$ at 81 K. (*C*), No domain structure observed at 300 K for $x = 0.20$ or in an undoped sample ($x = 0$). SEM primary beam: 10 kV and 10 pA. (*D*), Averaged tunneling $I(V)$ curves and derivative conductance (dI/dV) curves measured in bright and dark bubble domains. An energy gap is seen in tunneling $I(V)$ curve of dark domain where the current is reduced to the noise level (±1 pA). The gap is further confirmed by dI/dV data, where a differential conductance is essentially zero inside the gap. (*E*), Local resistance as a function of temperature measured using four-probe STM across a 5 μm stripe that falls into a single domain below 81 K. SEM images in *A*, *B*, and *C* are in the same magnification.

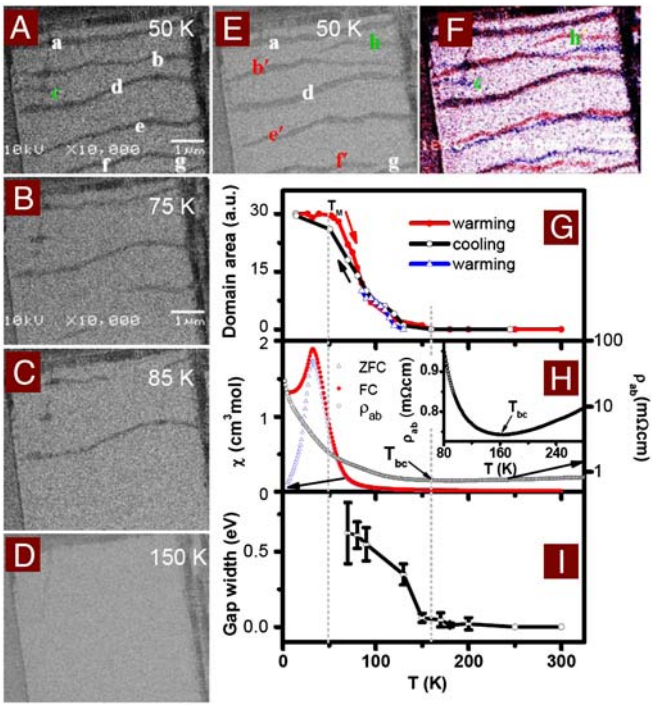

Fig. 2. *T*-dependent phase percolations in a $Sr_3(Ru_{0.8}Mn_{0.2})_2O_7$. (*A–E*), Domain images measured at various *T* for the same sample location. SEM primary beam: 10 kV, 10 pA. (*F*), Superimposed view of images *A* and *E*, shown in *blue* and *purple* respectively. (*G*). Domain areal change with *T* in the cleaved surface. (*H*), Resistivity ρ_{ab} and dc magnetic susceptibility χ as a function of *T* for bulk crystal. Inset: zoom-in of $\rho_{ab}(T)$ curve near MIT point. (*I*), The energy gap width as a function of *T* measured by STS. The energy gap is averaged over a (50×50 nm^2) region that is dark below 150 K and becomes bright at higher temperatures.

regions. Therefore, the SEM contrast observed here reflects the electronic state difference between dark and bright regions that correspond to insulating and metallic phases, respectively.

Indeed, SEM is capable of registering contrast between electronic phases according to their work functions (20). The resistance (R) of the microscopic local regions has been measured as a function of temperature (T) using four-probe STM across a 5 μm stripe. Although it starts melting above 81 K, the local MIT occurs near 135 K (Fig. 1*E*), below which R increases with decreasing T and reaches more than five orders of magnitude higher resistance at 10 K than that for its metallic state. Between 81 and 135 K, the single stripe turns into multiple disconnected stripes with smaller sizes, which vanish completely when reaching 135 K. Note that there is a kink in local R at $T \sim 90$ K (see Fig. 1*E*). This is likely due to the leakage current path through the surrounding conductive matrix when the insulating stripe domains shrink (see Fig. S2).

The phase domains can be tuned by changing temperature. Fig. 2*A–E* displays a few snapshot SEM images of stripe domains at different T. When warming up the sample from 50 K (Fig. 2*A*), the stripes melt gradually with T and disappear completely at around 150 K (Fig. 2*D*). Upon cooling down to 50 K again, stripes *a*, *d*, and *g* reappear as shown in Fig. 2*E*, but stripe *c* is missing and *h* is added, and stripes *b′*, *e′*, and *f′* are displaced from their original locations. The domain pattern changes can be seen more clearly in Fig. 2*F* where images of Fig. 2*A* and *E* are superimposed in blue and purple colors, respectively.

Remarkably, the evolution of competing phase domains correlates quantitatively with the change of macroscopic physical properties. A quantitative analysis of the domain areal change in a region of 30×30 μm^2 with temperature is displayed in Fig. 2*G*. On warming from 10 K, the stripe areal fraction remains largely unchanged up to $T_M \sim 50$ K. It is followed by a steep drop to zero at $T_c \sim 160$ K. On cooling from room temperature, the domain areal change essentially follows the same trace of the warming curve with little hysteresis. The bulk electrical resistivity (see the inset of Fig. 2*H*) shows a gradual MIT at $T_{bc} \sim 160$ K, coinciding well with the domain percolation process (see Fig. 2*G*). Note that the temperature below which domain areal change saturates corresponds to the AFM ordering temperature near T_M. In Fig. 2*H*, the magnetic susceptibility taken at both zero field cooling and field cool conditions reveals that the system undergoes AFM transition near $T_M = 50$ K. The magnetic susceptibility has a sharp increase prior to the formation of long-range AFM order, due to strong magnetic fluctuation. When the system forms true long-range AFM ordering, the total susceptibility decreases. As a result, the susceptibility increases below about 80 K and then decreases below about 30 K in Fig. 2*H*. This is consistent with previous assessment that the high temperature metal and the low temperature insulator in $Sr_3(Ru_{1-x}Mn_x)_2O_7$ correspond to PM and AFM phases respectively (16, 17), although the MIT occurs at much higher temperature than that of magnetic ordering.

The above analyses indicate that the macroscopic MIT of $Sr_3(Ru_{0.8}Mn_{0.2})_2O_7$ is a manifestation of microscopic phase competition and the domain percolation. Due to the percolating Mott transition nature, metal-insulator transition temperature (T_c) obtained from individual domains is not necessarily identical to that for the bulk (T_{bc}). This is corroborated by the observation in Fig. 1*E* where a local MIT appears at ~135 K, lower than the bulk T_{bc} value of 160 K. It is further confirmed by the evolution of the energy gap shown in Fig. 2*I*. The onset temperature of such gap opening varies from domain to domain and this percolation process leads to a globally continuous MIT transition. The global percolation transition temperature, where a "conductive"

network of insulating phase forms, would correspond to the bulk MIT (T_{bc}) in this case, and the Mott transition temperature in individual domains is associated with defects and strain field as discussed below. Note that although the bulk MIT appears at 160 K, SEM images on the surface still show a dominant metallic region in Figs. 1 and 2. The reasons are the following: First, as $T_c < T_{bc}$, it is possible for SEM to show a metallic surface while the bulk is still an insulator within the temperature window between T_c and T_{bc};Second and more importantly, the ability of SEM to resolve phase domains is limited both by the system spatial resolution (10 nm) and the current leakage path, thus the SEM will not be able to resolve small insulating domains in a metallic matrix. SEM contrast here reflects an electrical charging effect in insulating domains (details in *SI Text*). Due to the leakage paths of the metallic matrix surrounding the insulating domains, small insulating domains will not be able to change the SEM yield and only large insulating domains can be seen.

For complex systems involving chemical doping, theoretical simulation predicts that the chemical disorder introduced by impurity substitutions can form large-scale PS (21). However, the chemical-doping-induced PS would occur at the same location although the shape of the phase is not necessarily the same in different thermal cycles. While pure electronic interactions can also induce inhomogeneity in the charge density distribution, it would have random distribution at the nanoscale (3). Thus the electronic interaction and chemical disorder alone cannot fully explain the above observations in Fig. 2*F*. In order to gain insight into the origin of PS near the MIT, we explore the strain effect on phase domains and percolation by applying mechanical stress. While strain is often introduced by utilizing epitaxial lattice mismatch or hydrostatic pressure (14, 22), the former suffers from the complications induced by variations in defect structure and composition between different films and the latter renders the direct visualization of competing phases impractical. With a piezoelectric sample holder, we can apply a uniaxial compressive stress in the *ab* plane and image the evolution of phase domains in situ. Fig. 3*A* and *B* shows the domain patterns before and after applying strain, respectively (for temporal evolution, see Movie S1). The insulating domain appears brighter than the metallic matrix, inverted from the contrast in Figs. 1 and 2. This contrast inversion is due to an electron charging effect in the insulating regions. For a metal, the energy barrier (work function) for secondary electron emission is closely related to its Fermi energy. However, for an insulator, charge carriers can be trapped in the surface area, which can severely shift surface bands and thus change the work function and even lead to contrast inversion (Figs. S3–S5). Such a contrast inversion corroborates the coexistence of metal and insulator phases near the Mott transition.

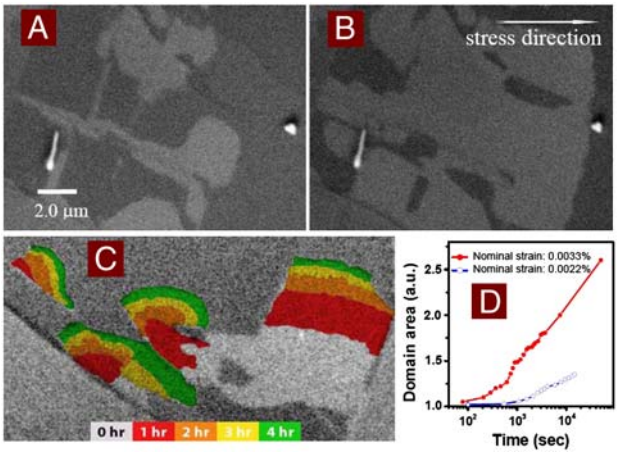

Fig. 3. Strain-induced domain evolutions in the cleaved surface of a $Sr_3(Ru_{0.8}Mn_{0.2})_2O_7$ at 81 K. (*A*), Domain image before stress and (*B*), after applying an uniaxial compressive stress in the *ab* plane (along the *a* axis) for 14 h with nominal strain of 0.0033%. (*C*), Domain evolution in time with nominal strain of 0.0022%. (*D*), Domain area change with time. SEM primary beam: 5 kV, 50 pA.

Our images shown in Fig. 3*B* and *C* clearly reveal that, in the presence of stress, the insulating phase expands dramatically at the expense of the metal one at a constant temperature. The domain growth is faster along the stress direction than that normal to the stress direction (Fig. 3*B*). The bubble and stripe shapes of domains displayed in Fig. 1 may thus reflect the local distributions of residual strain in the cleaved surface. As suggested theoretically for the manganites, lattice distortions and long-range strains can play an important role in determining the electronic properties of correlated systems (7, 23). According to theoretical simulation for manganites, the electron-lattice interactions can lead to local energetically favorable configurations and electronic PS over micrometer scales in the presence of strain, induced either externally (stress) or internally (chemical substitution) (7). Our real-space images in ruthenates provide unique direct evidence for this scenario. As shown in Fig. 3*B*, application of 0.0033% strain, deduced from the displacement of the piezoelectric holder, doubles the insulating domain area. As a result, the bulk resistivity increases by 120%. The "gigantic" response of the phase domains to the strain field in $Sr_3(Ru_{0.8}Mn_{0.2})_2O_7$ can stem from the interplay between the spatially confined Mn 3*d* orbitals and the extended, yet anisotropic, Ru 4*d*–O 2*p* electronic backbone of the Ru-O host. Owing to a smaller ionic radius, the Mn substitution for Ru creates an octahedral compression (16, 26), which alters the relative energies of *d* orbitals and enhances AFM ordering with a possibly orbitally ordered state at low *T* (17). A minute amount of external strain superimposes onto the distortions induced by Mn substitution, thus resulting in a "gigantic" response in insulating domains in $Sr_3(Ru_{0.8}Mn_{0.2})_2O_7$.

It is noted that the insulating domains expand slowly over a period of several hours, as shown in Fig. 3*C* for the crystal under constant strain field. Fig. 3*D* is a plot of time versus domain area in semilogarithmic scale. The domain area increases logarithmically with time without any sign of saturation in a 10 h duration. The speed of evolution apparently increases with increasing the amplitude of strain. Such behavior is reminiscent of diffuse phase transitions seen in Cr-doped $Nd_{1/2}Ca_{1/2}MnO_3$ (27) and $PbMg_{1/3}Nb_{2/3}O_3$ (28). The slow phase transition in these systems was explained using the random field model based on the stability consideration of the ordered state under a quenched random field (29). In Cr-doped $Nd_{1/2}Ca_{1/2}MnO_3$, partial substitution of Cr for Mn provides the quenched random field that destroys the orbital ordering (27). In $PbMg_{1/3}Nb_{2/3}O_3$ nanoscale ferroelectric domains embedded in a paraelectric matrix are sources of quenched random electric fields (27, 28). In the case of $Sr_3(Ru_{0.8}Mn_{0.2})_2O_7$, the doping of Mn introduces a local strain field, and the quenched disorder leads to PS. In this scenario, the order parameter is the orbital orientation, which is consistent with the previous suggestions that the AFM low-*T* phase has a long-range orbital order (16, 17).

Materials and Methods

We grew single crystals of $Sr_3(Ru_{1-x}Mn_x)_2O_7$ using the floating zone technique (15). The crystals (*ca.* $4 \times 5 \times 1$ mm^3) were cleaved in UHV at room temperature. The sample with a freshly cleaved surface was then transferred to four-probe STM chamber without breaking the UHV. The surface was first examined with single-tip STM to confirm the *ab* plane (Fig. S1) and then investigated by using a UHV (pressure $< 1 \times 10^{-10}$ torr) field emission SEM as well as STS. The local electrical transport was measured with the four-point contact method using the four-probe STM at variable temperature. The incident electron beam from SEM was blanked off during the STM, STS, and transport measurements. In the four-probe STM measurements, a "hard" contact that applies a mechanical stress to the sample surface has been avoided by controlling the tip-sample distance using STM feedback mechanism with a precision of subangstroms.

ACKNOWLEDGMENTS. We thank Elbio R. Dagotto, David C. Joy, and Jiandi Zhang for stimulating discussions. This research at Oak Ridge National Laboratory's Center for Nanophase Materials Sciences was sponsored by the Scientific User Facilities Division and Division of Materials Science and Engineering, Office of Basic Energy Sciences, U.S. Department of Energy. This work was also partially supported by a Department Of Energy Grant DE-SC0002136 (to E.W.P.).

1. Imada M, Fujimori A, Tokura Y (1998) Y. Metal-insulator transitions. *Rev Mod Phys* 70:1039–263.
2. Dagotto E (2005) Complexity in strongly correlated electronic systems. *Science* 309:257–262.
3. Dagotto E, Hotta T, Moreo A (2001) Colossal magnetoresistant materials: The key role of phase separation. *Phys Rep* 344:1–153.
4. Orenstein J, Millis AJ (2000) Advances in the physics of high-temperature superconductivity. *Science* 288:468–474.
5. Uehara M, Mori S, Chen CH, Cheong SW (1999) Percolative phase separation underlies colossal magnetoresistance in mixed-valent manganites. *Nature* 399:560–563.
6. Zhang LW, Israel C, Biswas A, Greene RL, de Lozanne A (2002) Direct observation of percolation in a manganite thin film. *Science* 298:805–807.
7. Ahn KH, Lookman T, Bishop AR (2004) Strain-induced metal-insulator phase coexistence in perovskite manganites. *Nature* 428:401–404.
8. Pan SH, et al. (2001) Microscopic electronic inhomogeneity in the high-Tc superconductor $Bi_2Sr_2CaCu_2O_{8+\delta}$. *Nature* 413:282–285.
9. Lang KM, et al. (2002) Imaging the granular structure of high-Tc superconductivity in underdoped $Bi_2Sr_2CaCu_2O_{8+\delta}$. *Nature* 415:412–416.
10. Hanaguri T, et al. (2004) A "checkerboard" electronic crystal state in lightly hole-doped $Ca_{2-x}Na_xCuO_2Cl_2$. *Nature* 430:1001–1005.
11. Ki-Seok K (2006) Bandwidth-control versus doping-control Mott transition in the Hubbard model. *Phys Rev B* 74:115122.
12. Hanaguri T, et al. (2004) STM/STS study of metal-to-Mott-insulator transitions. *Physica C* 408:328–329.
13. Ruddlesden SN, Popper P (1958) The compound $Sr_3Ti_2O_7$ and its structure. *Acta Crystallogr* 11:54–55.
14. Ikeda S-I, Maeno Y, Nakatsuji S, Kosaka M, Uwatoko Y (2000) Ground state in $Sr_3Ru_2O_7$: Fermi liquid close to a ferromagnetic instability. *Phys Rev B* 62:R6089–R6092.
15. Stone MB, et al. (2006) Temperature-dependent bilayer ferromagnetism in $Sr_3Ru_2O_7$. *Phys Rev B* 73:174426.
16. Mathieu R, et al. (2005) Impurity-induced transition to a Mott insulator in $Sr_3Ru_2O_7$. *Phys Rev B* 72:092404.
17. Hossain MA, et al. (2008) Crystal-field level inversion in lightly Mn-doped $Sr_3Ru_2O_7$. *Phys Rev Lett* 101:016404.
18. Kim T-H, et al. (2007) A cryogenic Quadraprobe scanning tunneling microscope system with fabrication capability for nanotransport research. *Rev Sci Instrum* 78:123701.
19. Zeng C, Kent PRC, Kim T-H, Li A-P, Weitering HH (2008) Charge-order fluctuations in one-dimensional silicides. *Nat Mater* 7:539–542.
20. Goldstein J, et al. (2003) *Scanning Electron Microscopy and x-Ray Microanalysis* (Kluwer Academic/Plenum Publishers, New York), 3rd Ed, pp 88–98.
21. Moreo A, Yunoki S, Dagotto E (1999) Solid state physics—phase separation scenario for manganese oxides and related materials. *Science* 283:2034–2040.
22. Biswas A, et al. (2001) Strain-driven charge-ordered state in $La_{0.67}Ca_{0.33}MnO_3$. *Phys Rev B* 63:184424.
23. Millis AJ (1998) Lattice effects in magnetoresistive manganese perovskites. *Nature* 392:147–150.
24. Shaked H, Jorgensen JD, Chmaissem O, Ikeda S, Maeno Y (2000) Neutron diffraction study of the structural distortions in $Sr_3Ru_2O_7$. *J Solid State Chem* 154:361–367.
25. Sushko YV, et al. (2004) Hydrostatic pressure effects on the magnetic susceptibility of ruthenium oxide $Sr_3Ru_2O_7$: Evidence for pressure-enhanced antiferromagnetic instability. *Solid State Commun* 130:341–346.
26. Cao G, et al. (2005) Itinerant ferromagnetism to insulating antiferromagnetism: A magnetic and transport study of single crystal $SrRu_{1-x}Mn_xO_3$ ($0 \leq x < 0.60$). *Phys Rev B* 71:035104.
27. Kimura T, Tomioka Y, Kumai R, Okimoto Y, Tokura Y (1999) Diffuse phase transition and phase separation in Cr-doped $Nd_{1/2}Ca_{1/2}MnO_3$: A Relaxor Ferromagnet. *Phys Rev Lett* 83:3940–3943.
28. Westphal V, Kleemann W, Glinchuk MD (1992) Diffuse phase-transitions and random-field-induced domain states of the "relaxor" ferroelectric $PbMg_{1/3}Nb_{2/3}O_3$. *Phys Rev Lett* 68:847–850.
29. Imry Y, Ma S-K (1975) Random-field instability of the ordered state of continuous symmetry. *Phys Rev Lett* 35:1399–1401.